

## Identification of Phase Transitions and Metastability in Dynamically Compressed Antimony Using Ultrafast X-Ray Diffraction

A. L. Coleman,<sup>1,2,\*</sup> M. G. Gorman,<sup>1,2</sup> R. Briggs,<sup>1,2</sup> R. S. McWilliams,<sup>1</sup> D. McGonegle,<sup>3</sup> C. A. Bolme,<sup>4</sup> A. E. Gleason,<sup>4,5</sup> D. E. Fratanduono,<sup>2</sup> R. F. Smith,<sup>2</sup> E. Galtier,<sup>6</sup> H. J. Lee,<sup>6</sup> B. Nagler,<sup>6</sup> E. Granados,<sup>6</sup> G. W. Collins,<sup>7</sup> J. H. Eggert,<sup>2</sup> J. S. Wark,<sup>3</sup> and M. I. McMahon<sup>1</sup>

<sup>1</sup>*SUPA, School of Physics and Astronomy, and Centre for Science at Extreme Conditions, The University of Edinburgh, Edinburgh EH9 3FD, United Kingdom*

<sup>2</sup>*Lawrence Livermore National Laboratory, 7000 East Avenue, Livermore, California 94500, USA*

<sup>3</sup>*Department of Physics, Clarendon Laboratory, Parks Road, University of Oxford, Oxford OX1 3PU, United Kingdom*

<sup>4</sup>*Shock and Detonation Physics, Los Alamos National Laboratory, P.O. Box 1663, Los Alamos, New Mexico 87545, USA*

<sup>5</sup>*Department of Geological and Environmental Sciences, Stanford University, Stanford, California 94305, USA*

<sup>6</sup>*Linac Coherent Light Source (LCLS), SLAC National Accelerator Laboratory, Menlo Park, California 94025, USA*

<sup>7</sup>*Department of Mechanical Engineering, University of Rochester, 235 Hopeman Building, P.O. Box 270132, Rochester, New York 12647, USA*



(Received 23 May 2018; published 28 June 2019)

Ultrafast x-ray diffraction at the LCLS x-ray free electron laser has been used to resolve the structural behavior of antimony under shock compression to 59 GPa. Antimony is seen to transform to the incommensurate, host-guest phase Sb-II at  $\sim 11$  GPa, which forms on nanosecond timescales with ordered guest-atom chains. The high-pressure bcc phase Sb-III is observed above  $\sim 15$  GPa, some 8 GPa lower than in static compression studies, and mixed Sb-III/liquid diffraction are obtained between 38 and 59 GPa. An additional phase which does not exist under static compression, Sb-I', is also observed between 8 and 12 GPa, beyond the normal stability field of Sb-I, and resembles Sb-I with a resolved Peierls distortion. The incommensurate Sb-II high-pressure phase can be recovered metastably on release to ambient pressure, where it is stable for more than 10 ns.

DOI: [10.1103/PhysRevLett.122.255704](https://doi.org/10.1103/PhysRevLett.122.255704)

Under dynamic compression, antimony is a classic phase-transforming element [1]. Of particular note has been the anomalously long transition time of 2–3 ns determined for the shock-induced phase transition at 8.8 GPa [1–3]. Shock compression studies of antimony to date have typically used explosively generated shock waves, and the existence of phase transitions has been inferred from measurements of the shock wave profiles [1–5], where complex, multiple wave structures greatly complicated the analysis.

The room-temperature phase transition sequence in antimony under static compression has been determined in detail using x-ray diffraction. Antimony crystallizes in the  $A7$  structure [Sb-I, space group  $R\bar{3}m$ , atom on  $(0,0,u)$  with  $u = 0.234$ ] at ambient conditions, which is a Peierls-distorted simple-cubic (sc) structure. On compression, the  $c/a$  ratio of Sb-I decreases as the distortion relaxes, and a sc phase (where  $c/a = \sqrt{6}$  and  $u = \frac{1}{4}$ ) is approached. While early studies reported a transition to the sc phase (hereafter Sb-I') at  $\sim 7$  GPa [6–8], later diffraction studies [9–11] showed that this phase is not obtained, but rather that Sb-I transforms to an incommensurate host-guest (HG) structure at  $\sim 8$  GPa [11]. This phase, Sb-II, then persists up to 28.8 GPa at 300 K, where it then transforms to the

body-centered cubic (bcc) structure of Sb-III. Recent diffraction studies have observed a modest temperature effect on the transformation pressures [12].

The absence of a suitably bright, short-pulsed x-ray source has long prevented a similar level of detail being obtained in shock compressed samples. However, x-ray free electron lasers (XFELs) now provide 50 fs pulses of monochromatic x rays that are ideal for structural studies of dynamically compressed matter. Here we report a study utilizing laser compression and x-ray pulses from the Linac Coherent Light Source (LCLS) XFEL to study the structural behavior of shock compressed Sb to 59 GPa. We find that, in contrast to static-compression studies, Sb-I' is obtained via a fast (nanosecond or less) phase transition from Sb-I at 7.9 GPa. Diffraction profiles from Sb-I' differ markedly from those from Sb-I, and they can be fitted equally well by either a sc structure with distorted Debye-Scherrer (DS) rings arising from the sample strength or a rhombohedral structure with  $c/a \leq \sqrt{6}$ . Shock compression to higher pressures results in further transitions—to the incommensurate Sb-II phase at 11.3 GPa, to the bcc Sb-III phase at 14.6 GPa, and to the liquid phase above 37.6 GPa. All of these transitions take place on nanosecond timescales or less, as seen in Bi and Sc [13,14]. On pressure release

from the high-pressure phases, we find, for the first time, that the incommensurate phase can be recovered metastably to ambient pressures, where it has a lifetime of more than 10 ns.

Experiments were performed at the matter in extreme conditions (MEC) end station of the LCLS [15]. Ablation-driven shock waves were generated using a Nd:glass optical laser (527 nm, 20 ns, quasi-flat-topped pulses [16]) and were used to compress the target package which consisted of a 50- $\mu\text{m}$ -thick polyimide ablator and a 10- $\mu\text{m}$ -thick, deposited Sb layer. Additional data were collected using targets with a 500- $\mu\text{m}$ -thick LiF window affixed to their rear [14]. The monochromatic pulses provided by the LCLS ( $\lambda = 1.240 \text{ \AA}$ ) were focused to a 50  $\mu\text{m}$  diameter spot and then centered on the variable diameter (150–500  $\mu\text{m}$ ) focal spot of the drive laser. The x rays and optical laser were then centered on the target.

X-ray diffraction data were collected by an array of Cornell-SLAC pixel array detectors (CSPADs) arranged in a transmission Debye-Scherrer geometry [17]. The 2D diffraction patterns from the individual detectors were integrated azimuthally and combined to produce 1D diffraction profiles extending from  $2\theta = 18$  to  $101^\circ$ . A velocity interferometer system for any reflector (VISAR) diagnostic was used to both quantify the spatial planarity of the shock across the region of the target upon which the x rays were incident and measure the rear surface velocity of the Sb in order to determine the shock breakout time and to calculate the pressure within the target via the Rankine-Hugoniot equations [14,17,24].

Unless explicitly stated, all x-ray data were collected on compression, that is, prior to the shock front reaching the rear surface of the Sb layer. Diffraction data were collected on compression, both with and without LiF windows, between 1.9 and  $\sim 59$  GPa. The as-grown Sb samples comprised longitudinally oriented grains  $\sim 500$  nm in diameter [17] and were highly textured, as revealed by the azimuthal variations in the intensity of DS rings (see Fig. S1 [17]). In marked contrast to the behavior we observed previously in shocked Sc [14], sample texture persisted in both the compressed Sb-I and high-pressure phases. The sample was found, at ambient pressure, to have a fiber texture with the rhombohedral  $c$  axis parallel to the sample normal; the texture was not characterized for the higher pressure phases.

Sb-I was seen on compression up to 6.9 GPa, with the Peierls distortion (as determined from the  $c/a$  axial ratio) reducing much more rapidly with pressure than has been reported previously in static compression studies [17]. On further compression to 7.9 GPa, the diffraction pattern from the compressed sample simplified greatly, as shown in Fig. 1, and could be fitted with a simple cubic structure. This undistorted cubic structure is not obtained in the most recent static compression studies, but our results show that it can be created on nanosecond timescales via shock compression.

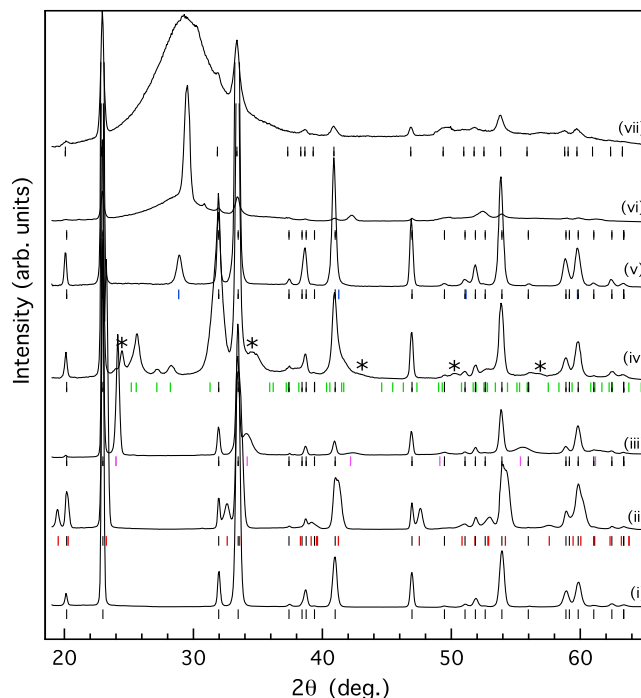


FIG. 1. Integrated profiles from shock compressed Sb as a function of the pressure. The colored tick marks beneath each profile show the calculated peak positions for the structures at those pressures, while the black tick marks beneath profiles (ii)–(vii) locate the peaks from the uncompressed Sb-I ahead of the shock front. The diffraction profiles are from (i) Sb-I (A7) at ambient pressure; (ii) compressed Sb-I at 1.9 GPa (red); (iii) Sb-I' fitted as simple cubic Sb without strength at 7.9 GPa (pink); (iv) Sb-II (HG) at 12.0 GPa (green); (v) Sb-III (bcc) at 18.9 GPa (blue); (vi) bcc/liquid Sb at 37.6 GPa; and (vii) liquid Sb at 57.2 GPa. Asterisks in profile (iv) mark peaks from Sb-I'.

Although the spacing of the Sb-I' peaks indicated a cubic structure, profile (iii) in Fig. 1 shows small but distinct displacements of several calculated peak positions from those observed in the integrated profile. An analysis of the 2D diffraction images revealed small azimuthal variations in the  $d$  spacings of the DS rings, suggesting the cubic phase exhibited some small degree of strength (i.e., anisotropic strain) [17]. We quantified this using the methods described in Ref. [25], and this revealed that the distortion of DS rings could indeed be explained by a cubic structure exhibiting strength [17].

However, the textured nature of the DS rings, and the incomplete azimuthal coverage of the Cornell-SLAC pixel array detectors (see Fig. S1 [17]), meant that a second structure, rhombohedral A7 with  $u = \frac{1}{4}$  and  $c/a$  slightly less than  $\sqrt{6}$ , could not be excluded [17]. Had it been possible to collect the full 2D diffraction pattern, then these two models would have been distinguishable [17]. Unfortunately, those areas of the 2D diffraction images where distinct differences in the diffraction patterns would be seen were not covered by the detectors.

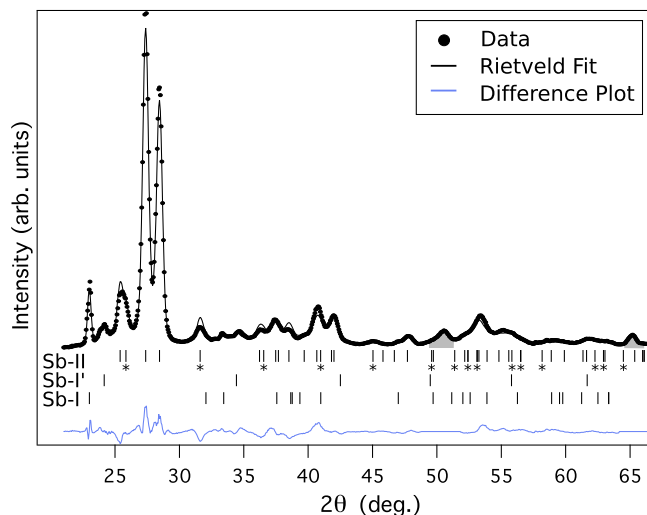


FIG. 2. A three-phase (Sb-I, Sb-I', and Sb-II) Rietveld fit to a diffraction profile of Sb obtained on release from  $\sim 17$  GPa, for a Sb/LiF sample ( $R_p = 6.0\%$ ,  $wR_p = 6.7\%$ ,  $\text{GoF} = 1.12$ , and  $R(F^2) = 3.4\%$ —see Table S1 [17]). The calculated peak positions for Sb-I, Sb-I' (fitted as simple cubic), and Sb-II are shown by markers below the profile. The guest peaks from the HG phase, identified by starred tick marks, confirm the guest chains are ordered. The gray shaded areas show two additional, unidentified peaks omitted from the three-phase fit.

On further compression above 11.3 GPa, the appearance of a completely different diffraction pattern signaled a transition to the Sb-II phase. While the DS rings from this phase still exhibit azimuthal variations in intensity, they are undistorted and exhibit no detectable effects of strain. Figure 2 shows a Rietveld fit to an almost single-phase diffraction pattern from incommensurate Sb-II obtained on release, 5 ns after the shock wave had entered the LiF window on the rear of the target. It is estimated that the subsequent release of the Sb sample to match impedance with the LiF would take  $\sim 4$  ns. The pressure of the Sb sample immediately before the arrival of the shock at the LiF interface was  $\sim 17$  GPa, lowering to  $\sim 14$  GPa after release. This indicates that the sample had released from the higher-pressure bcc phase (obtained above 14.6 GPa; see below), back into the HG phase. The refined parameters of the Sb-II structure, utilizing superspace group  $I'4/mcm(00\gamma)000s$ , were  $a_H = 7.983(3)$  Å,  $c_H = 3.859(3)$  Å, and  $\gamma = 1.305(5)$  [ $V/V_0 = 0.767(1)$ ]. The refined atomic coordinates for the host and guest atoms at the same pressure are  $(0.153(1), x + \frac{1}{2}, 0)$  and  $(0,0,0)$ , respectively. These parameters are in excellent agreement with those obtained previously in a static compression study at 14.5 GPa and 300 K [26]. In contrast to the HG phase we observed in Sc under shock compression [14], the “guest-only” Bragg peaks that arise from scattering from only the guest atoms of the HG structure are clearly visible, as highlighted in Fig. 2, showing that structures of the complexity of Sb-II can form completely in a nanosecond, with fully ordered incommensurate chains.

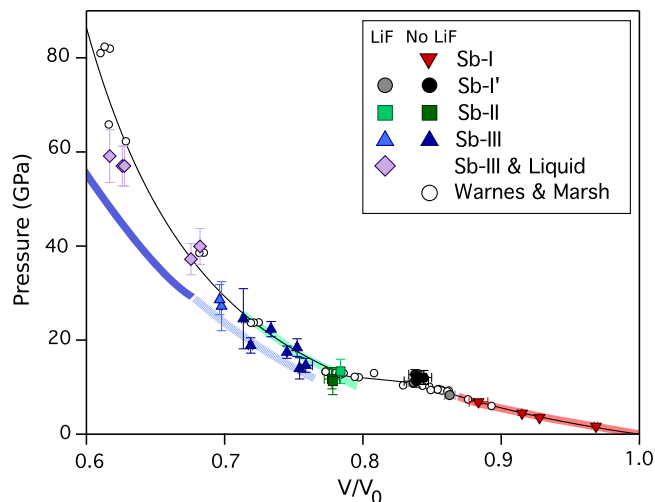


FIG. 3. The volumetric compression of Sb. Hugoniot equation of state (EOS) data obtained in this study are shown using colored symbols, and points obtained using a LiF backing window are shown using lighter shaded symbols. The unfilled symbols show the previous shock compression data collected by Warnes and Marsh [3,27]. The solid line through the data is calculated using two linear shock velocity ( $U_s$ ) and particle velocity ( $u_p$ ) relations ( $U_s = 1.36u_p + 2.50$  below 10.6 GPa and  $U_s = 1.65u_p + 1.93$  above 12.3 GPa), as detailed in Supplemental Material [17]. The blue, green, and red shaded lines show the isothermal compression of Sb-III, Sb-II, and Sb-I, respectively, at 300 K [26]. The compressibility of Sb-III has been extrapolated below 28.8 GPa (shown as a lighter line) using a third-order Birch-Murnaghan EOS with  $K' = 4$ .

Further data collected late on free-surface release from targets without LiF windows also showed, in addition to Sb-I, diffraction peaks from the HG phase, with lattice parameters  $a_H = 8.295$  Å,  $c_H = 4.007$  Å, and  $\gamma = 1.308$  [ $V/V_0 = 0.860(3)$ ], slightly smaller than the values expected at ambient pressure [11,28]. However, the same lattice parameters were obtained from data collected 6, 8, and 10 ns after the initiation of release, providing evidence that the HG phase was at ambient pressure in each case. The HG phase was not observed in data collected more than 14 ns after release, placing an upper time limit on its stability at ambient pressure. This is the first time that a high-pressure incommensurate phase has been recovered to ambient pressure and highlights the opportunities for transiently recovering exotic high-density phases to ambient conditions [29].

On increasing the drive pressure further, we observed a transition to the high-pressure bcc Sb-III phase at 14.6 GPa, much lower than the static compression transition pressure of 28.8 GPa at 300 K [26] (Fig. 3) and 20 GPa at the on-Hugoniot temperature of  $\sim 900$  K [12] (Fig. 4). At 37.6 GPa, diffraction from liquid Sb was first observed. The relative weakness of the liquid scattering compared to that from bcc [profile (vi) in Fig. 1] suggests that melting had just initiated at this pressure. The bcc and liquid phases

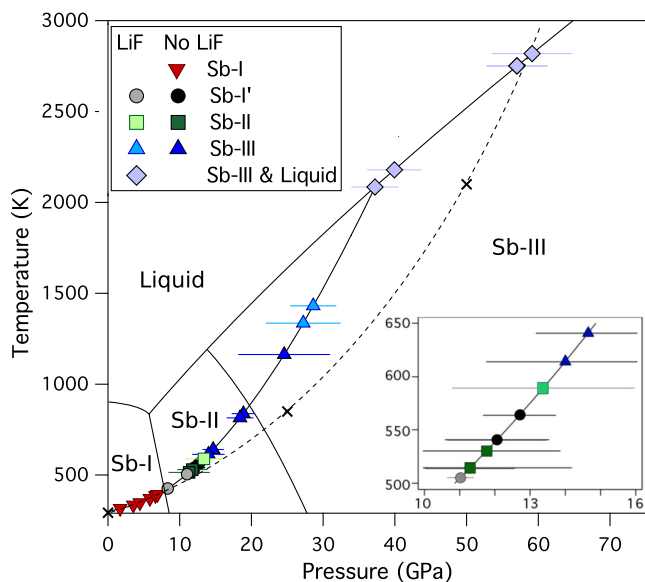


FIG. 4. The equilibrium phase diagram of Sb [12], along with the phases observed on compression in this study along the estimated Hugoniot [17]. The melting curve is given by a Simon-Glatzel fit to previously observed melting curve data [30,31] and the first LCLS data point in which liquid diffraction is observed. All other data points obtained from partially melted samples are plotted on this estimated melt curve. Black crosses indicate Hugoniot points calculated in a previous gas-gun study, with a dashed line included as a guide to the eye [5].

were found to coexist between 37.6 and 59.2 GPa, where the sample has almost completely melted [profile (vii) in Fig. 1]. The Hugoniot and melting curve are therefore coincident over this pressure range.

Figure 4 shows, for comparison, a series of Hugoniot points from a previous gas-gun study [5]. These data, along with subsequent published datasets, are included in our PT-Hugoniot calculations (as discussed in Supplemental Material [17]). Differences between the two calculated PT-Hugoniots shown in Fig. 4 arise from differences in thermodynamic variables used in the temperature calculations.

The observation of the Sb-I' phase, the transition pressure of 11.3 GPa to the HG phase, and the transition pressure of only 14.6 GPa to the bcc phase are all strikingly different from the behavior seen in static-compression studies of Sb at 300 K. In such studies, the Sb-I' phase is not observed, and the transitions to the HG and bcc phases occur at 8.6 and 28.8 GPa, respectively [9,26]. As our shock compression data were collected on the Hugoniot at elevated temperatures, it is possible that these different transition pressures arise simply from the different temperature regimes of the studies. However, we have recently conducted a high-temperature static compression study of Sb to 31 GPa and 835 K [12], the measured and extrapolated phase boundaries from which are shown in Fig. 4. It is evident that the different behaviors seen in Sb under shock and static compression cannot be explained

simply by the temperature differences but must arise from the compression method. There is no evidence of the Sb-I' phase on static compression, and the shock-induced transition to Sb-I' occurs at a very similar pressure to the Sb-I  $\rightarrow$  Sb-II transition observed under static compression. This suggests that Sb-I' is a metastable extension of the Sb-I phase, accessed only via dynamic compression on the nanosecond timescales.

The calculations of Wang *et al.* have highlighted the existence of transitions from the "normal" rhombohedral  $A7$  structure to other  $A7$  variants in the vicinity of the Sb-I  $\rightarrow$  Sb-II transition [32]. Specifically, they reported structural instabilities at 5.7 and 6.6 GPa to variants whose energy difference was so small ( $\leq 2$  meV/cell) that the 5.7–6.6 GPa pressure range should be considered as a region of coexistence. While these  $A7$  variants were not seen in our recent static compression study [12], Wang *et al.* stated that transitions to them could be induced by the presence of a substantial uniaxial stress component along the  $c$  axis. As the microstructure of our deposited Sb layers comprises columnar grains (Fig. S5 [17]), whose  $c$  axes are aligned perpendicular to the layer, the crystallites are therefore compressed along their  $c$  axes by the shock wave, providing the uniaxial stress component considered by Wang *et al.* It is noticeable that the diffraction patterns from Sb-I' are the only ones exhibiting the distorted DS rings that indicate a nonhydrostatic stress state. Further study would be required to confirm whether the Sb-I' phase is also observed under dynamic compression in samples exhibiting a different crystal orientation.

The observation of the transition to the bcc Sb-III phase at only 14.6 GPa is very surprising, given the transition pressure of  $\sim 23$  GPa seen in static compression studies at 650 K [12] and the transition pressure of 26.8 GPa determined from electronic structure calculations [28]. While transition pressures are often increased (overdriven) under dynamic compression [1] due to kinetic hinderance, the degree of *underdriving* we see in Sb is unusual, particularly as diffraction enables us to establish that the transition is to the same Sb-III structure seen in other studies. Our data suggest that transitions to cubic phases are favored in Sb under dynamic pressure loading; this is a behavior that has recently been reported in shock compressed Bi [33]. Further study is needed to investigate whether this is also true for other materials that form complex structures under static compression.

Finally, we return to the identity of the "slow" shock-induced phase transition reported previously above 8.8 GPa, with a volume change consistent with that found here for the Sb-I'  $\rightarrow$  Sb-II phase transition [1,2]. The reported transition pressure sits squarely within the stability field established for Sb-I', and the reported transition time of 2–3  $\mu$ s is 2 orders of magnitude longer than our experimental timescales. However, the strong variation of transition pressure with sample thickness [3] suggests

that the transition pressure in our 10- $\mu\text{m}$ -thick samples would be much closer to the observed Sb-I'  $\rightarrow$  Sb-II transition pressure of 11.3 GPa. We would also expect to observe the transition on a much shorter timescale in our experiment: Studies of the  $\alpha - \epsilon$  phase transition in iron have reported that shock stress and target thickness can cause a significant variation in the transition time [34,35]. The two-wave structure we see at  $\sim 12$  GPa (as shown in Fig. S3 [17]) is similar to that observed by Warnes [3] in conjunction with a phase transition and is observed here in all samples where both Sb-I' and Sb-II are present in the diffraction patterns on compression. This enables us to establish that the previously observed transition, where the large volume reduction results in two-wave compression, arises from the Sb-I'  $\rightarrow$  Sb-II transition, with a transition time decreasing from microsecond to nanosecond time-scales for increasing applied stress.

In conclusion, using x-ray diffraction at an XFEL, we have been able to successfully observe and resolve the phase behavior of shock compressed Sb up to 59 GPa. We see a transition to Sb-I' at 7.9 GPa, a phase not seen in previous studies but which calculations suggest might arise as a result of uniaxial compression. This phase appears where the Sb-II host-guest structure forms under equilibrium conditions [12], as shown in Fig. 4. A transition to Sb-II, with ordered guest chains, is found to occur on nanosecond timescales at 11.3 GPa, more than 3 GPa higher than in static compression studies, and this phase can be recovered to ambient pressure, where it is metastable for more than 10 ns. Sb-II is found to be stable to only 13.9 GPa, above which the cubic Sb-III phase is observed,  $\sim 8$  GPa lower than its expected equilibrium transformation pressure of 23 GPa [12]. Sb-III remains the stable solid phase to 59 GPa, with melting beginning above 37.6 GPa.

Formation of the incommensurate Sb-II phase is thus strongly impeded on compression, with a new metastable phase (Sb-I') forming in its place, and the back transformation is impeded on release. There is also an anomalous underdriving of the transition to the higher-pressure Sb-III phase, at conditions where Sb-II is expected at equilibrium. This suggests a large kinetic barrier exists between the incommensurate host-guest structure and the structures of Sb-I, Sb-I', and Sb-III, all of which are cubic or slight distortions thereof, leading to the formation of metastable states. The resulting underdriving of a high-pressure transition stands in contrast to the expectation that kinetic effects cause only overdriving of phase transformations under dynamic compression [1]. Thus, at most pressures where Sb-II is stable under equilibrium conditions, we observe other phases that are energetically less favorable but which are more structurally accessible from the initial rhombohedral phase.

Our results clearly highlight both the differences in material properties which may arise as a consequence of compression technique and subsequent strain rates and the

consequent importance of examining the detailed dynamic phase-transformation behavior, which in this case differs considerably to that expected from studies at near-equilibrium conditions. Sb shows marked differences in structural behavior between static and shock compression, especially in the dramatic contraction of the stability region of Sb-II in the latter, making the establishment of a universal phase diagram for Sb challenging. A study of these phase transitions using pressure loading mechanisms with intermediate characteristic sample strain rates (such as dynamic-DAC [36] or ramp compression [37]) may elucidate how the kinetic and energetic transformation landscape evolves between equilibrium and ultrafast compression.

M. I. M. and J. S. W. acknowledge support from the Engineering and Physical Sciences Research Council (EPSRC) under Grant No. EP/J017256/1 and EP/J017051/1. R. S. M. acknowledges support from EPSRC under Grant No. EP/P024513/1. D. M. is grateful to the Atomic Weapons Establishment for support. The work by J. H. E., D. E. F., R. F. S., D. C. S., G. W. C., A. L. C., M. G. G., and R. B. was performed under the auspices of the U.S. Department of Energy by Lawrence Livermore National Laboratory under Contract No. DE-AC52-07NA27344. C. A. B. acknowledges support from Science Campaign 2 at Los Alamos National Laboratory, which is operated for the National Nuclear Security Administration of the U.S. Department of Energy under Contract No. DE-AC52-06NA25396. Use of the Linac Coherent Light Source (LCLS), SLAC National Accelerator Laboratory, is supported by the U.S. Department of Energy, Office of Science, Office of Basic Energy Sciences under Contract No. DE-AC02-76SF00515. The matter in extreme conditions instrument is supported by the U.S. Department of Energy, Office of Science, Office of Fusion Energy Sciences under Contract No. SF00515. We thank Carol A. Davis and Paul Mirkirimi of Lawrence Livermore National Laboratory for their help in preparing the Sb targets. Also we thank Zeiss for their assistance in imaging the surface of the Sb samples. Finally, we extend our sincere thanks to the referees for their many useful comments and guidance.

---

\*Corresponding author.  
coleman55@llnl.gov

- [1] G. E. Duvall and R. A. Graham, *Rev. Mod. Phys.* **49**, 523 (1977).
- [2] B. R. Breed and D. Venable, *J. Appl. Phys.* **39**, 3222 (1968).
- [3] R. H. Warnes, *J. Appl. Phys.* **38**, 4629 (1967).
- [4] R. E. Duff and F. S. Minshall, *Phys. Rev.* **108**, 1207 (1957).
- [5] R. G. McQueen and S. P. Marsh, *J. Appl. Phys.* **31**, 1253 (1960).
- [6] L. F. Vereschagin and S. S. Kabalkina, *Sov. Phys. JETP* **20**, 274 (1965).
- [7] T. N. Kolobyanina, S. S. Kabalkina, L. F. Vereschagin, and L. V. Fedina, *Sov. Phys. JETP* **28**, 88 (1969).

- [8] S. S. Kabalkina, T. N. Kolobyanina, and L. F. Vereschagin, *Sov. Phys. JETP* **31**, 259 (1970).
- [9] D. Schiferl, *Rev. Sci. Instrum.* **48**, 24 (1977).
- [10] H. Iwasaki and T. Kikegawa, *Physica (Amsterdam)* **139–140(B+C)**, 259 (1986).
- [11] O. Degtyareva, M. I. McMahon, and R. J. Nelmes, *Phys. Rev. B* **70**, 184119 (2004).
- [12] A. L. Coleman, M. Stevenson, M. I. McMahon, and S. G. Macleod, *Phys. Rev. B* **97**, 144107 (2018).
- [13] M. G. Gorman, R. Briggs, E. E. McBride, A. Higginbotham, B. Arnold, J. H. Eggert, D. E. Fratanduono, E. Galtier, A. E. Lazicki, H. J. Lee, H. P. Liermann, B. Nagler, A. Rothkirch, R. F. Smith, D. C. Swift, G. W. Collins, J. S. Wark, and M. I. McMahon, *Phys. Rev. Lett.* **115**, 095701 (2015).
- [14] R. Briggs *et al.*, *Phys. Rev. Lett.* **118**, 025501 (2017).
- [15] B. Nagler *et al.*, *J. Synchrotron Radiat.* **22**, 520 (2015).
- [16] D. C. Swift and R. G. Kraus, *Phys. Rev. E* **77**, 066402 (2008).
- [17] See Supplemental Material at <http://link.aps.org/supplemental/10.1103/PhysRevLett.122.255704> for additional information on the experimental procedure, the pressure determination, the Hugoniot model, the texture of the samples, the Sb-I' structural models, and comparison with static data, which includes Refs. [18–23].
- [18] P. Hart, S. Boutet, G. Carini, M. Dubrovin, B. Duda, D. Fritz, G. Haller, R. Herbst, S. Herrmann, C. Kenney *et al.*, *Proc. SPIE Int. Soc. Opt. Eng.* **8504**, 85040C (2012).
- [19] A. E. Gleason, C. A. Bolme, H. J. Lee, B. Nagler, E. Galtier, D. Milathianaki, J. Hawreliak, R. G. Kraus, J. H. Eggert, D. E. Fratanduono, G. W. Collins, R. Sandberg, W. Yang, and W. L. Mao, *Nat. Commun.* **6**, 8191 (2015).
- [20] Antimony (sb) debye temperature, heat capacity, density, melting point, *Non-Tetrahedrally Bonded Elements and Binary Compounds I*, Datasheet from Landolt-Börnstein—Group III Condensed Matter Vol. 41c, edited by O. Madelung, U. Rössler, and M. Schulz (Springer-Verlag, Berlin, 1998).
- [21] G. V. Bunton and S. Weintraub, *J. Phys. C* **2**, 116 (1969).
- [22] D. McGonegle, D. Milathianaki, B. A. Remington, J. S. Wark, and A. Higginbotham, *J. Appl. Phys.* **118**, 065902 (2015).
- [23] J. M. Brown and R. G. McQueen, *J. Geophys. Res.* **91**, 7485 (1986).
- [24] P. M. Celliers, D. K. Bradley, G. W. Collins, D. G. Hicks, T. R. Boehly, and W. J. Armstrong, *Rev. Sci. Instrum.* **75**, 4916 (2004).
- [25] A. Higginbotham and D. McGonegle, *J. Appl. Phys.* **115**, 174906 (2014).
- [26] O. Degtyareva, M. I. McMahon, and R. J. Nelmes, *High Press. Res.* **24**, 319 (2004).
- [27] S. P. Marsh, *LASL Shock Hugoniot data*, Los Alamos Series on Dynamic Material Properties (University of California, Berkeley, 1980).
- [28] U. Häussermann, K. Söderberg, and R. Norrestam, *J. Am. Chem. Soc.* **124**, 15359 (2002).
- [29] J. Sun, D. D. Klug, and R. Martoňák, *J. Chem. Phys.* **130**, 194512 (2009).
- [30] S. M. Stishov and N. A. Tikhomirova, *Sov. Phys. JETP* **48**, 1215 (1965).
- [31] W. Klement, A. Jayaraman, and G. C. Kennedy, *Phys. Rev.* **131**, 632 (1963).
- [32] X. Wang, K. Kunc, I. Loa, U. Schwarz, and K. Syassen, *Phys. Rev. B* **74**, 134305 (2006).
- [33] M. G. Gorman *et al.*, *Sci. Rep.* **8**, 16927 (2018).
- [34] B. J. Jensen, G. T. Gray III, and R. S. Hixson, *J. Appl. Phys.* **105**, 103502 (2009).
- [35] R. F. Smith, J. H. Eggert, D. C. Swift, J. Wang, T. S. Duffy, D. G. Braun, R. E. Rudd, D. B. Reisman, J. P. Davis, M. D. Knudson, and G. W. Collins, *J. Appl. Phys.* **114**, 223507 (2013).
- [36] Z. Konôpková, A. Rothkirch, A. K. Singh, S. Speziale, and H.-P. Liermann, *Phys. Rev. B* **91**, 144101 (2015).
- [37] A. Lazicki, J. R. Rygg, F. Coppari, R. Smith, D. Fratanduono, R. G. Kraus, G. W. Collins, R. Briggs, D. G. Braun, D. C. Swift, and J. H. Eggert, *Phys. Rev. Lett.* **115**, 075502 (2015).